Reports on Geodesy and Geoinformatics, 2025, Vol. 120, pp. 96–100

DOI: 10.2478/rgg-2025-0020
Received: 8 November 2025 / Accepted: 9 December 2025
Published online: 15 December 2025

ORIGINAL ARTICLE

GNSS sites at Hornsund reveal increase of land uplift rate due to recent acceleration of deglaciation at Svalbard

Marcin Rajner [1]

[1]Faculty of Geodesy and Cartography, Warsaw University of Technology, pl. Politechniki 1, 00-661 Warszawa, Poland

marcin.rajner@pw.edu.pl

Abstract

This paper discusses recent and up-to-date uplift rates at Polish Polar Station at Hornsund (SW Svalbard). Twenty years of continuous Global Navigation Satellite Systems (GNSS) measurements was used to infer contemporary vertical crust deformation due to viscous and elastic response to variable loads. Using environmental models good agreement of observed land uplift with numerical predictions was found. Most of the vertical change stem from Glacial Isostatic Adjustment (GIA), Little Ice Age (LIA) and Present Day Ice Melting (PDIM). Significant increase of uplift was observed in the last few years from 9.0 mm yr^{-1} up to 11.5 mm yr^{-1}. This can be attributed to increase of ice mass loss at Svalbard archipelago of additional 10 Gt yr^{-1}. In case of GNSS site at Hornsund 80 % of PDIM comes from melting of glaciers at south Spitsbergen.

Key words: GNSS, ice mass budget, Svalbard, land uplift

1 Introduction

The ongoing global warming is one of the greatest challenge in recent history of human mankind (Fischer and Knutti, 2015). This problem gained a lot of attention and is subject of many strong opinions. The main role for geosciences is to provide non-opinionated, reliable information of this phenomenon. It is a tremendous work to synthesize all collected data to show the full picture. This is very hard to achieve, but any additional information matters. One of the most spectacular and impressive effect is ice mass loss in polar regions (Stroeve et al., 2011). It has serious impact globally through sea level rise (Gardner et al., 2013) and recent studies indicates its self increase (Wunderling et al., 2020).

Ice mass balance can be measured with many different techniques depending on time and geographical scale (Shepherd et al., 2012). Geodesy plays special role in this interdisciplinary unification techniques. Direct methods like satellite altimetry or repeated Global Navigation Satellite Systems (GNSS) field measurements gives a precise, location oriented, information of ice mass budget. Indirect methods complete this studies giving estimates usually at much larger scale. Satellite gravimetry is such an indirect, non-positional method which was applied for many regions including Svalbard (Mémin et al., 2011). Measuring land uplift, as the indicator of crust load, is other, relatively easy, achievable method to infer variation of mass distribution (Jiang et al., 2013). This technique was successfully used for Svalbard in the past (Kierulf et al., 2009, 2021, 2022; Rajner, 2018).

A new GNSS installations were installed in 2020 at Hornsund Polish Polar Station which provide contribution to global data and analysis centres. History of permanent GNSS at Hornsund is much longer, though. This paper present uniformly reprocessed 20 years of data with emphasize on land uplift rates and its cause, mainly regional ice mass loss. The recent findings show significant increase of uplift velocity reaching level of 11.5 mm yr^{-1}. This clearly indicates acceleration of ice mass loss at south Svalbard.

2 Study area

The Svalbard archipelago is located in Arctic (Fig. 1), has area of 61×10^3 km^2 and more than 60 % is covered with ice (Fig. 6). Due to its location and availability, it is place for numerous observatories,

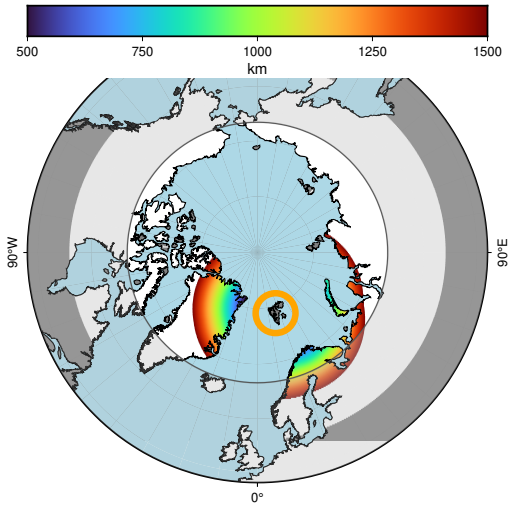

Figure 1. Location of Svalbard and distances to other land masses

laboratories and scientific expeditions. Ny-Ålesund (at the north) is important core geodetic observatory combining many techniques like Very Large Baseline Interferometry (VLBI), GNSS, Superconducting Gravimetry (SG) and Absolute Gravimetry (AG) to name the most important ones (Kierulf et al., 2009; Omang and Kierulf, 2011). Permanent GNSS sites NYAL and NYA1 have one of the longest time series within International GNSS Service (IGS) community. A few other sites at Svalbard have time series reaching back to 2010 (Kierulf et al., 2021, 2022; Omang and Kierulf, 2011). In recent years more GNSS installation for different purposes were installed or are in planning phase.

Svalbard has important unique feature in loading studies, as it is far from other land masses (Fig. 1). Therefore, almost all uplift from Present Day Ice Melting (PDIM) comes from Svalbard exclusively.

3 GNSS data

On the south on Spitsbergen, at the Polish Polar Station at Hornsund (see Fig. 6), GNSS permanent measurements are taken since 2005 (Rajner, 2018). It is operated by Institute of Geophysics (IGF) Polish Academy of Sciences (PAS). Firstly this receiver served only as a reference site for field measurements (Rajner, 2010; Błaszczyk et al., 2024). First location named ASTR (old astronomical measurements site) is presented in Fig. 2a. Due to obstacles in satellites visibility, and in order to mitigate multipath errors, in late 2009 it was moved to better location several tens of meters from its origin, hereafter this location is referred as HORN (Hornsund). During expedition of Warsaw University of Technology (WUT) in 2020 a new multi system GNSS equipment was installed. A new receiver WUTH (WUT Hornsund) replaced HORN, and another one PPSH (Polish Polar Station Hornsund) was installed on a new monument (Fig. 2b). Table 1 summarizes main technical information of these installations.

Both PPSH and WUTH data are now easily available through International organizations listed in Tab. 1. Full details of current setup can be found in the detailad conventional logs https://epncb.oma.be/pub/station/log/ppsh00nor_20231001.log, https://epncb.oma.be/pub/station/log/wuth00nor_20240903.log.

(a) ASTR, 2006

(b) PPSH (left antenna) and WUTH (right antenna), 2020

Figure 2. GNSS permanent sites at Hornsund

To end up with complete picture of GNSS measurements at Hornsund a mention to other receivers dedicated for ionosphere and reflectometry research is needed. These receivers have shorter measurement history, and are mounted in a way which exclude them from geodynamics studies. Their length is also limitation in terms of geodynamics studies presented in this paper.

3.1 Processing

The all available data described in Section 3 was processed to obtain daily results of position change. This was done with GipsyX (Bertiger et al., 2020) scientific software along with precise final orbits provided by Jet Propulsion Laboratory (JPL). The ephemeris used were given in IGS20 terrestrial reference frame and processing was performed in Precise Point Positioning (PPP) mode. The conventional models for earth tides, ocean tidal loading and individual antenna calibration (for PPSH and WUTH) was applied. The atmospheric loading was not considered, as for the islands this effect is usually very small, and of less of importance in long term estimates. The resulting time series in geocentric Cartesian coordinate were converted to horizontal frame and only variations of height are subject of this paper. Rajner (2018) gave results for selection of data collected for thtis study, but with much shorter time span. All data, archive and new one, was reprocessed using most up-to-date software and models.

3.2 Trend estimation

Estimation of the time series parameters was done using Hector (v.2.1) software (Bos et al., 2013).[1] This package is designated to estimate trends along with seasonal signals in time series with temporally correlated noise. It employs Maximum Likelihood Estimation (MLE) method under hood, and can handle gaps correctly. Hector can simultaneously estimate offsets in time series, therefore we constructed one long time series composing ASTR, HORN and WUTH data, in order to analyse long term changes of land uplift.

Table 1. Summary of GNSS permanent measurements at Hornsund

site	since	until	receiver	antenna	satellite systems	network
ASTR	2005.06.26	2009.09.09	Leica GRX1200	LEIAT504	GPS	
HORN	2009.09.09	2020.09.07	Leica GRX1200	LEIAT504	GPS	
PPSH	2020.09.07		Leica GR25	LEIAR20/LEIM	GPS+GLO+GAL	IGS, EPN, EPOS
WUTH	2020.09.07		SEPT POLARX5S	SEPCHOKE B3E6/SPKE	GPS+GLO+GAL+BDS+SBAS	EPN, EPOS

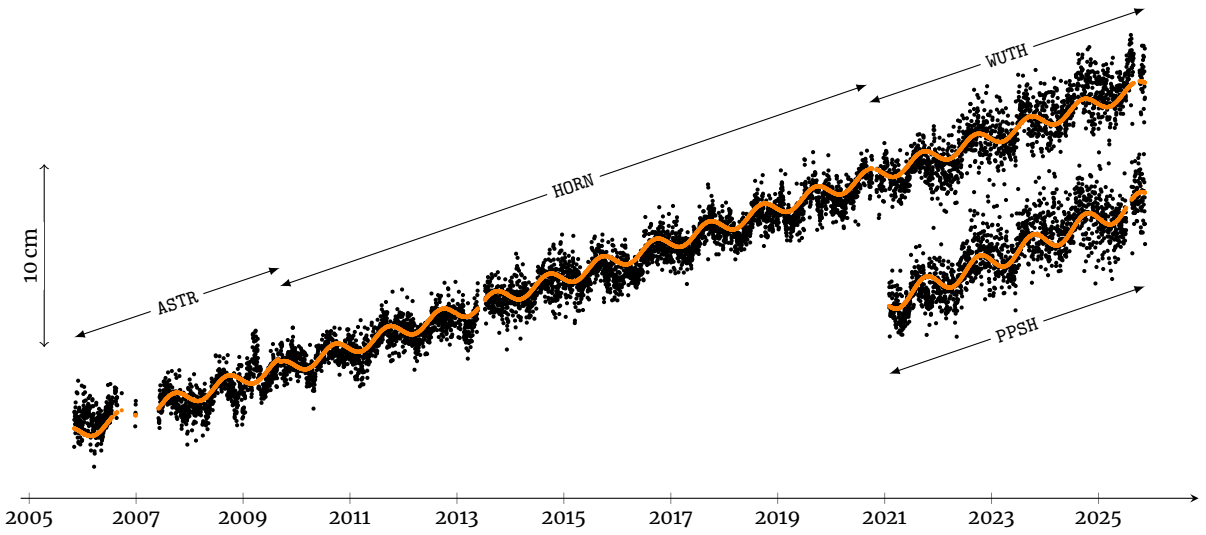

Figure 3. Height time series of ASTR, HORN, WUTH and PPSH; the offsets in 2009 and 2020 were determined within trend estimation step; dots represents daily solution of each site and orange line is best fitted linear and seasonal signal; the difference between WUTH and PPSH is not in scale to improve readability

4 Results

Figure 3 represents height variation of GNSS sites at Hornsund over last two decades. We used rigorously estimated offset to fit ASTR, HORN and WUTH as one long time series. Offsets equal to 8108.47 mm and 84.86 mm for $H_{\mathrm{HORN}} - H_{\mathrm{ASTR}}$ and $H_{\mathrm{WUTH}} - H_{\mathrm{HORN}}$ respectively was found. On this plot absolute difference of height between PPSH and WUTH is not at scale, and these values are shifted to make comparison easier. A few prominent features are visible and are discussed in next subsections.

4.1 Long term vertical movement

We can clearly see in Fig. 3 a long term uplift at the level of 1 cm yr^{-1}. This dominant change is similar for each GNSS site and its subtle changes are subject of section 4.3. Most of this uplift comes from Glacial Isostatic Adjustment (GIA), Little Ice Age (LIA) and PDIM combined. Rajner (2018) gave numbers for GIA (1.1 mm yr^{-1}, Peltier et al. (2015)) and LIA (4.0 mm yr^{-1}, Mémin et al. (2014)) at Hornsund. We used that values in this study, as this effect does not vary much in time.

4.2 Seasonal variation

In Figure 4 we present time series of height changes for PPSH and WUTH where linear trend was extracted. This gives more insight of seasonal height variation. The two recently installed sites exhibit similar behaviour. This duplication reinforces our conclusions of geophysical nature of this signal.

The seasonal loading cycle driven by accumulation and melting period is also distinctive feature in Figures 3 and 4. Amplitudes of 5 mm were found to be in overall good agreement to those presented by Kierulf et al. (2021). We observed amplitude increase from 4.5 mm at the beginning of GNSS measurements to 5.5 mm in last few years. This indicates increase of seasonal ice and snow transport in Svalbard cryosphere. Increase of summer mass loss (with

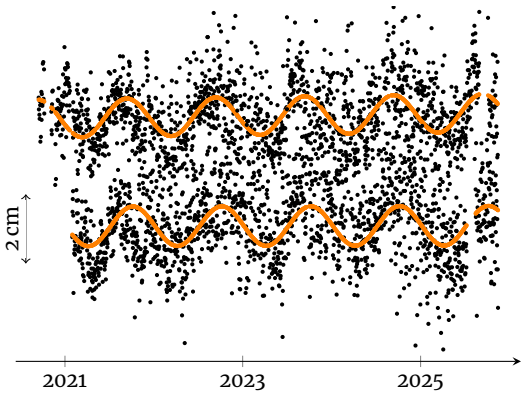

Figure 4. Seasonal variability of height of WUTH (upper) and PPSH (lower); dots represents daily GNSS estimates and orange line best fitted seasonal signal, linear trend was removed, absolute values were shifted to improve readability

1 available through teromovigo company https://teromovigo.com/product/hector

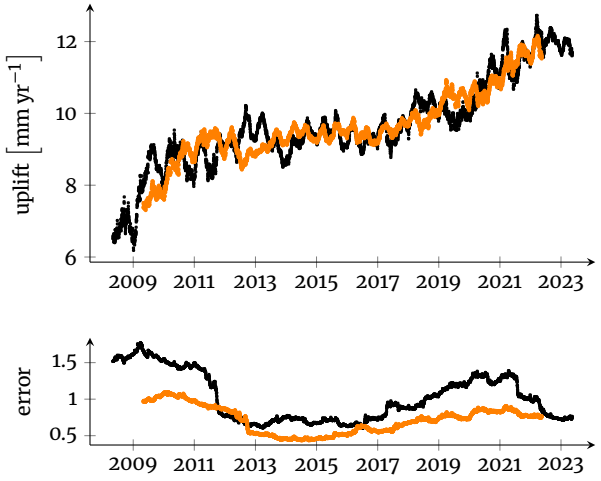

Figure 5. Uplift rate computed using sliding window with width of 5 years (black) and 7 years (orange); each dot represents value for center of this time span; values of computed uplift rates are given in upper graph and the uncertainties are given in bottom graph respectively

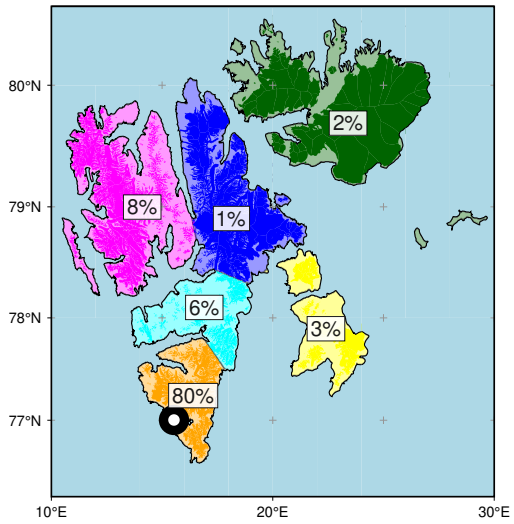

Figure 6. Effect of PDIM on uplift rate at Hornsund (circle) divided by different Svalbard zones; different colours depict different regions; dark color shows glaciated areas

extreme year 2024) was recently reported by Schuler et al. (2025) what supports our findings of increasing amplitude of seasonal loading.

4.3 Variation of uplift rate

Processing of PPSH and WUTH has shown uplift rate significantly larger than previously reported. Rajner (2018) gave value of 8 mm yr^{-1} for period of 2006 – 2016. Here we found that uplift rates are much higher than previously reported, i.e. mean value for whole considered time span was equal to 9.5 mm yr^{-1}. For ASTR–HORN epoch it was equal to 9 mm yr^{-1} while both PPSH and WUTH gave value of 11.5 mm yr^{-1} for last 5 years.

Rajner (2018) evaluated PDIM impact using numerical mass balance model from Aas et al. (2016). This model was estimating roughly a 9 Gt yr^{-1} of mass loss over a period of 2003-2013 causing elastic uplift of 2.1 mm yr^{-1} at Hornsund. Additional ice mass loss of 6 Gt yr^{-1} had to be applied to fit GNSS uplift rates at the end of 2016. Rough estimate indicate that we will need another 10 Gt yr^{-1} of mass loss to fit the current uplift rates. In total, our new, coarse estimate, indicates a mass loss of 25 Gt yr^{-1} over Svalbard.

In order to track uplift rate long term variation we applied moving window to time series constructed with measurements from ASTR, HORN and WUTH with offset corrected. The results are shown in Figure 5. Rajner (2018) already reported increase of uplift rate after year 2011. This was done based on visual inspection on time series. We apply different method here, computing separately uplift rate for each window of selected time width. Five, and seven years, was used, which was long enough to smooth short time variation caused by measurements and processing deficiencies, but still leaving long term changes. Blewitt and Lavallée (2002) stated already that it is necessary to use at least 2.5 years for linear trend estimation in GNSS networks. For rapid changes with very high seasonal amplitudes this width seemed to leave too much noise, though.

In Figure 5 we can observe two important uplift increase during measurement period. First one ends in 2011 and other one started at 2019. One should note that inferring exact dates is improper as we use five years width moving window. This recent speed up is significant and this is agreement with recent finding of increased melting down of Svalbard glaciers in resent years (Schuler et al., 2025).

Bottom graph of Figure 5 shows the determined uncertainties of estimated uplift rates using Hector software. Larger values in 2009 and 2020 are caused by offsets in time series due to equipment change. These values are still low enough to claim that GNSS time series indeed observe current increase of ice mass loss at Svalbard.

4.4 Regional discrimination of ice mass loss

We stated at the beginning the PDIM from outside of Svalbard can be neglected. Rajner (2018) estimated impact of Greenland to be less than 0.3 mm yr^{-1}. Using model of mass balance given by Aas et al. (2016), we computed realistic effects of PDIM of different, Svalbard regions. Technique presented by Farrell (1972) was used to computed loading deformations. Then impact of each region were computed separately. Figure 6 shows the specific numbers. We can state that about 80 % of uplift comes from mass balance from South Spitsbergen. This finding is important for future research, as many new GNSS installation already works, all will work in near future at Svalbard archipelago.

5 Conclusions

Using GNSS measurements from last two decades at Hornsund we found that elastic response due to PDIM increased significantly in recent years. The values of height changed from 7 mm yr^{-1} in 2009 to 9 mm yr^{-1} in mid 2010 years and increased to 11.5 mm yr^{-1} in the last few years. This can be attributed to additional 10 Gt yr^{-1} of mean ice mass loss at Svalbard. Almost 80 % of this effect comes from melting of glaciers at south Spitsbergen. This increase is with agreement with recent glaciological observations (Schuler et al., 2025).

We estimated indirectly that total ice mass loss is 25 Gt yr^{-1} using conventional models for GIA and LIA to extract this effects from uplift. The change of elastic response is good indicator of changes of ice mass loss. However, the quantitative assessment of ice mass loss will require future AG measurements, as discrimination of PDIM from disco-elastic effect can be made only by combination of position and gravity measurements (A et al., 2013).

References

A, G., Wahr, J., and Zhong, S. (2013). Computations of the viscoelastic response of a 3-D compressible Earth to surface loading: an application to Glacial Isostatic Adjustment in Antarctica and Canada. *Geophysical Journal International*, 192(2):557–572, doi:10.1093/gji/ggs030.

Aas, K. S., Dunse, T., Collier, E., Schuler, T. V., Berntsen, T. K., Kohler, J., and Luks, B. (2016). The climatic mass balance of Svalbard glaciers: a 10-year simulation with a coupled atmosphere–glacier mass balance model. *The Cryosphere*, 10(3):1089–1104, doi:10.5194/tc-10-1089-2016.

Bertiger, W., Bar-Sever, Y., Dorsey, A., Haines, B., Harvey, N., Hemberger, D., Heflin, M., Lu, W., Miller, M., Moore, A. W., Murphy, D., Ries, P., Romans, L., Sibois, A., Sibthorpe, A., Szilagyi, B., Vallisneri, M., and Willis, P. (2020). GipsyX/RTGx, a new tool set for space geodetic operations and research. *Advances in Space Research*, 66(3):469–489, doi:https://doi.org/10.1016/j.asr.2020.04.015.

Błaszczyk, M., Luks, B., Pętlicki, M., Puczko, D., Ignatiuk, D., Laska, M., Jania, J., and Głowacki, P. (2024). High temporal resolution records of the velocity of Hansbreen, a tidewater glacier in Svalbard. *Earth System Science Data*, 16(4):1847–1860, doi:10.5194/essd-16-1847-2024.

Blewitt, G. and Lavallée, D. (2002). Effect of annual signals on geodetic velocity. *Journal of Geophysical Research: Solid Earth*, 107(B7):ETG 9–1–ETG 9–11, doi:https://doi.org/10.1029/2001JB000570.

Bos, M. S., Fernandes, R. M. S., Williams, S. D. P., and Bastos, L. (2013). Fast error analysis of continuous GNSS observations with missing data. *Journal of Geodesy*, 87(4):351–360, doi:10.1007/s00190-012-0605-0.

Farrell, W. E. (1972). Deformation of the Earth by surface loads. *Reviews of Geophysics*, 10(3):761–797, doi:10.1029/RG010i003p00761.

Fischer, E. M. and Knutti, R. (2015). Anthropogenic contribution to global occurrence of heavy-precipitation and high-temperature extremes. *Nature Climate Change*, 5(6):560–564, doi:10.1038/nclimate2617.

Gardner, A. S., Moholdt, G., Cogley, J. G., Wouters, B., Arendt, A. A., Wahr, J., Berthier, E., Hock, R., Pfeffer, W. T., Kaser, G., Ligtenberg, S. R. M., Bolch, T., Sharp, M. J., Hagen, J. O., van den Broeke, M. R., and Paul, F. (2013). A Reconciled Estimate of Glacier Contributions to Sea Level Rise: 2003 to 2009. *Science*, 340(6134):852–857, doi:10.1126/science.1234532.

Jiang, W., Li, Z., van Dam, T., and Ding, W. (2013). Comparative analysis of different environmental loading methods and their impacts on the GPS height time series. *Journal of Geodesy*, 87(7):687–703, doi:10.1007/s00190-013-0642-3.

Kierulf, H. P., Kohler, J., Boy, J.-P., Geyman, E. C., Mémin, A., Omang, O. C. D., Steffen, H., and Steffen, R. (2022). Time-varying uplift in Svalbard—an effect of glacial changes. *Geophysical Journal International*, 231(3):1518–1534, doi:10.1093/gji/ggac264.

Kierulf, H. P., Plag, H.-P., and Kohler, J. (2009). Surface deformation induced by present-day ice melting in Svalbard. *Geophysical Journal International*, 179(1):1–13, doi:10.1111/j.1365-246X.2009.04322.x.

Kierulf, H. P., van Pelt, W. J. J., Petrov, L., Dähnn, M., Kirkvik, A.-S., and Omang, O. (2021). Seasonal glacier and snow loading in Svalbard recovered from geodetic observations. *Geophysical Journal International*, 229(1):408–425, doi:10.1093/gji/ggab482.

Mémin, A., Spada, G., Boy, J.-P., Rogister, Y., and Hinderer, J. (2014). Decadal geodetic variations in Ny-Ålesund (Svalbard): role of past and present ice-mass changes. *Geophysical Journal International*, 198:285–297, doi:10.1093/gji/ggu134.

Mémin, A., Rogister, Y., Hinderer, J., Omang, O. C., and Luck, B. (2011). Secular gravity variation at Svalbard (Norway) from ground observations and GRACE satellite data. *Geophysical Journal International*, 184(3):1119–1130, doi:10.1111/j.1365-246X.2010.04922.x.

Omang, O. C. D. and Kierulf, H. P. (2011). Past and present-day ice mass variation on Svalbard revealed by superconducting gravimeter and GPS measurements. *Geophysical Research Letters*, 38(22), doi:10.1029/2011GL049266. L22304.

Peltier, W. R., Argus, D. F., and Drummond, R. (2015). Space geodesy constrains ice age terminal deglaciation: The global ICE-6G_C (VM5a) model. *Journal of Geophysical Research: Solid Earth*, 120(1):450–487, doi:10.1002/2014JB011176. 2014JB011176.

Rajner, M. (2010). Some remarks on determining short-period changes in glacier surface velocity using GPS technique — case study of Hans glacier example. *Geodesy and Cartography*, 59(1):39–47, doi:10.2478/v10277-012-0007-8.

Rajner, M. (2018). Detection of ice mass variation using GNSS measurements at Svalbard. *Journal of Geodynamics*, 121:20–25, doi:10.1016/j.jog.2018.06.001.

Schuler, T. V., Benestad, R. E., Isaksen, K., Kierulf, H. P., Kohler, J., Moholdt, G., and Schmidt, L. S. (2025). Svalbard's 2024 record summer: An early view of Arctic glacier meltdown? *Proceedings of the National Academy of Sciences*, 122(34):e2503806122, doi:10.1073/pnas.2503806122.

Shepherd, A., Ivins, E. R., A, G., Barletta, V. R., Bentley, M. J., Bettadpur, S., Briggs, K. H., Bromwich, D. H., Forsberg, R., Galin, N., Horwath, M., Jacobs, S., Joughin, I., King, M. A., Lenaerts, J. T. M., Li, J., Ligtenberg, S. R. M., Luckman, A., Luthcke, S. B., McMillan, M., Meister, R., Milne, G., Mouginot, J., Muir, A., Nicolas, J. P., Paden, J., Payne, A. J., Pritchard, H., Rignot, E., Rott, H., Sørensen, L. S., Scambos, T. A., Scheuchl, B., Schrama, E. J. O., Smith, B., Sundal, A. V., van Angelen, J. H., van de Berg, W. J., van den Broeke, M. R., Vaughan, D. G., Velicogna, I., Wahr, J., Whitehouse, P. L., Wingham, D. J., Yi, D., Young, D., and Zwally, H. J. (2012). A Reconciled Estimate of Ice-Sheet Mass Balance. *Science*, 338(6111):1183–1189, doi:10.1126/science.1228102.

Stroeve, J. C., Serreze, M. C., Holland, M. M., Kay, J. E., Malanik, J., and Barrett, A. P. (2011). The Arctic's rapidly shrinking sea ice cover: a research synthesis. *Climatic Change*, 110(3–4):1005–1027, doi:10.1007/s10584-011-0101-1.

Wunderling, N., Willeit, M., Donges, J. F., and Winkelmann, R. (2020). Global warming due to loss of large ice masses and Arctic summer sea ice. *Nature Communications*, 11(1), doi:10.1038/s41467-020-18934-3.